

# FRACTURE TOUGHNESS OF WOOD AND WOOD COMPOSITES DURING CRACK PROPAGATION

*Noah Matsumoto*

Structural Analysis Engineer—Methods and Allowables  
Structures Technology  
The Boeing Company  
Mesa, AZ  
E-mail: yonoah@hotmail.com

*John A. Nairn*\*†

Professor and Richardson Chair  
Wood Science and Engineering  
Oregon State University  
Corvallis, OR  
E-mail: John.Nairn@oregonstate.edu

(Received December 2010)

**Abstract.** Mode I fracture toughness as a function of crack length of medium-density fiberboard (MDF), particleboard (PB), and Douglas-fir (DF) was measured using a new energy-based method. PB and MDF are examples of composites that develop fiber bridging during crack propagation, which causes their toughness to increase with crack length. Longitudinal cracks in DF also displayed fiber-bridging behavior, but only when the crack plane was normal to the tangential direction. MDF and PB experiments were performed for both in-plane and out-of-plane cracks. The toughness of the former was much higher than the latter. The in-plane crack toughness of MDF was higher than PB, but its out-of-plane toughness was lower. PB made using a new soy-based resin had an in-plane toughness similar to commercial PB but an out-of-plane toughness three times higher. Out-of-plane crack propagation is suggested as an improved method for measuring internal bond (IB) properties. When the fracture method was compared with conventional IB tests, both methods showed that the soy PB was better but the fracture method provided a clearer distinction.

**Keywords:** Fracture, fiber bridging, numerical modeling, *R* curves, IB tests.

## INTRODUCTION

Medium-density fiberboard (MDF), particleboard (PB), and Douglas-fir (DF) are three common building materials. MDF is composed of wood fibers commonly bonded together with a urea formaldehyde resin. PB is similar but made with wood particles, instead of fibers, and various resins, such as a recently developed, formaldehyde-free soy-based resin (Li et al 2004). DF is an important softwood species. Although DF is not a wood composite product, its internal biological structure makes it an anisotropic and heterogeneous material whose fracture properties are better studied

with composite material fracture methods than with conventional fracture methods for isotropic, homogeneous materials.

Wood or wood composite structural performance is often assessed by bending strength tests (modulus of rupture) (ASTM 2009a) and internal bond (IB) tests (ASTM 2009b). Experience in nonwood materials, however, suggests that fracture toughness is a better indicator of real-world performance than strength tests (Williams 1984). As such, fracture performance of wood and wood composites should be considered in wood design, but few tests are available.

Several factors contribute to composite fracture toughness, including its fiber or particles, their orientations, the resin or matrix, and properties of

\* Corresponding author

† SWST member

the interfaces. Measuring fracture toughness can be difficult in composites because they frequently develop process zones at the crack tip. In wood products, the process zone is typically a fiber-bridging zone comprised of nonfractured constituent materials in the wake of a propagating crack tip. In MDF and DF, fiber bridging consists of wood fibers that span the crack surface. In PB, it is wood particles. The zone can be small or large, but in wood products, it is generally large compared with typical laboratory-scale specimen dimensions. As a result, fiber bridging may influence the entire crack propagation process in laboratory-scale specimens.

Fiber bridging complicates fracture experiments on wood products. First, such zones invalidate traditional fracture mechanics methods (ASTM 2006). Those methods rely on precalculated calibration functions to find toughness (stress intensity factor) from failure load. Unfortunately, these functions assume stress-free fracture surfaces and thus are invalid for cracks with fiber-bridging stresses. Second, fiber bridging can make it difficult to visually identify the crack tip and to measure crack lengths; these lengths are needed for data reduction. Third, when fiber bridging is significant, toughness increases as the crack propagates (Nairn 2009). Fracture characterization of such materials requires continuous monitoring of toughness as a function of crack growth. The result is known as the *R* curve or fracture-resistance curve.

All fiber-bridging issues can be overcome by available fracture mechanics methods, albeit nonstandard ones. First, instead of using stress intensity methods requiring calibration functions, toughness can be measured using energy methods that find the energy release rate directly from experiments even in the presence of bridging zones (Matsumoto and Nairn 2009; Nairn 2009). Crack growth measurements needed for this method are made possible by measuring the strain field ahead of the crack tip using digital image correlation (DIC) methods (or full-field strain measurement techniques) (Sutton et al 1983). Shifts in this strain field with time imply an increment in crack growth (Matsumoto and

Nairn 2009). Finally, when applied to crack propagation experiments, these methods can measure the full *R* curve for the material (Matsumoto and Nairn 2009) rather than a single number.

The objective of this study was to use energy methods to measure toughness during crack propagation for MDF, PB, and DF and to study them for different crack growth directions. To study the role of the resin in toughness, experiments were performed on both conventional and soy resin PB. The resulting *R* curves were interpreted by numerical modeling (Nairn 2009) to derive toughness and bridging-effect information (ie bridging stress) for each material. Because MDF, PB, and DF are all anisotropic, crack growth was characterized in different directions. In MDF and PB, a crack plane perpendicular to the plane of the panel is called an in-plane crack (LT and TL), whereas a crack plane parallel to the plane of the panel is called an out-of-plane crack (ZT and ZL) (Fig 1). In DF, a longitudinal crack with its plane perpendicular to the growth rings is a tangential-longitudinal (TL) crack, whereas a crack with its plane tangential to the growth rings is a radial-longitudinal (RL) crack (Fig 1). All these crack orientations were studied.

#### MATERIALS AND METHODS

MDF panels were provided by Flakeboard (Springfield, OR) as  $1.2 \times 2.4$ -m (T  $\times$  L directions) panels at two densities, 609 and 737 kg/m<sup>3</sup> (38 or 46 lb/ft<sup>3</sup>), and in two thicknesses, 12.7 and 19.05 mm. Two types of PB were tested. One was a commercial PB with a urea formaldehyde resin (Roseburg Forest Products, Roseburg, OR; Missoula pine particles, thickness 19.48 mm, density 730 kg/m<sup>3</sup>) purchased at a local lumber store. The other was a research PB with a soy flour adhesive resin (Li et al 2004) (thickness 19.43 mm, density 653 kg/m<sup>3</sup>). Solid wood specimens were Select Structural I Douglas-fir free of knots (thickness 22.2-22.6 mm). Prior to testing, all specimens were conditioned at 20°C and 60% RH until equilibrium.

All fracture tests used the modified compact tension (CT) specimens shown in Fig 2. This

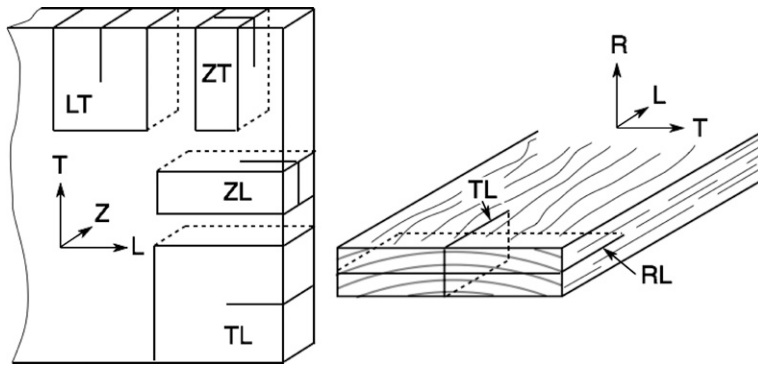


Figure 1. Crack planes in medium-density fiberboard and particleboard (left) and in Douglas-fir (right). Each crack is defined by two letters. The first letter is the direction normal to the crack plane; the second letter is the direction of crack propagation.

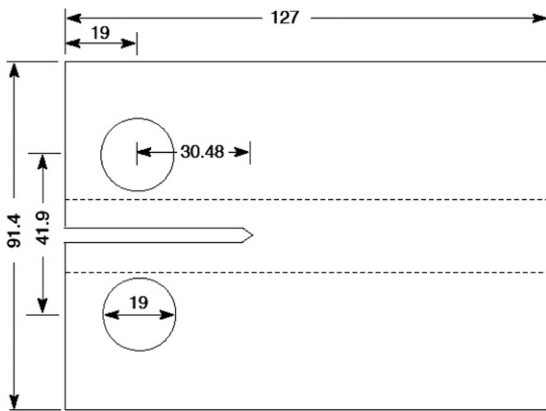


Figure 2. Elongated compact tension specimens used for all fracture experiments. All dimensions are in millimeters. Specimens were loaded by 19-mm steel pins in displacement control.

specimen was derived from the standard CT specimen (ASTM 2006) except elongated in the width direction from 95.25 to 127.0 mm to provide more room for crack propagation. Mode I loading was applied by steel pins at a constant displacement rate of 0.05 mm/min. In-plane MDF, PB, and DF CT specimens were cut from panels or boards. Out-of-plane MDF and PB CT specimens were built up by gluing ZT or ZL orientation slices (Fig 1) to arms cut from the main panel. By this method, all tests could be done with the same CT specimen geometry. The dashed lines in Fig 2 indicate the location of ZT or ZL slices for those specimens.

All fracture experiments used an energy-based method (Matsumoto and Nairn 2009; Nairn 2009). This technique enables direct measurement of energy release rate during crack propagation and contains data analysis methods developed to decrease scatter. In brief, specimens were monotonically loaded while recording force and crack length as functions of displacement (Fig 3a). Although some crack propagation methods periodically unload the specimen to measure energy, that approach cannot be used for materials with fiber bridging because it crushes the fibers in the process zone and changes the results (Atkins and Mai 1985). One option for measuring energy in materials with crack-plane interference is to assume unloading returns to the origin (if the process zone did not interfere). Indeed, recent experiments (Matsumoto and Nairn 2009) confirmed that this assumption is reasonable for MDF; in this study, it was assumed reasonable for PB and DF as well. Thus, the cumulative energy released as a function of displacement was measured by integrating the force-displacement curve up to each displacement and then subtracting the area under the assumed unloading curve (shaded area in Fig 3a). Cross-plotting this measured energy (per unit thickness) with measured crack length gives cumulative energy released as a function of crack length (Fig 3b). Finally, the slope of this curve is the energy release rate as a function of crack length (*R* curve). It was found by numerical differentiation (Fig 3c).

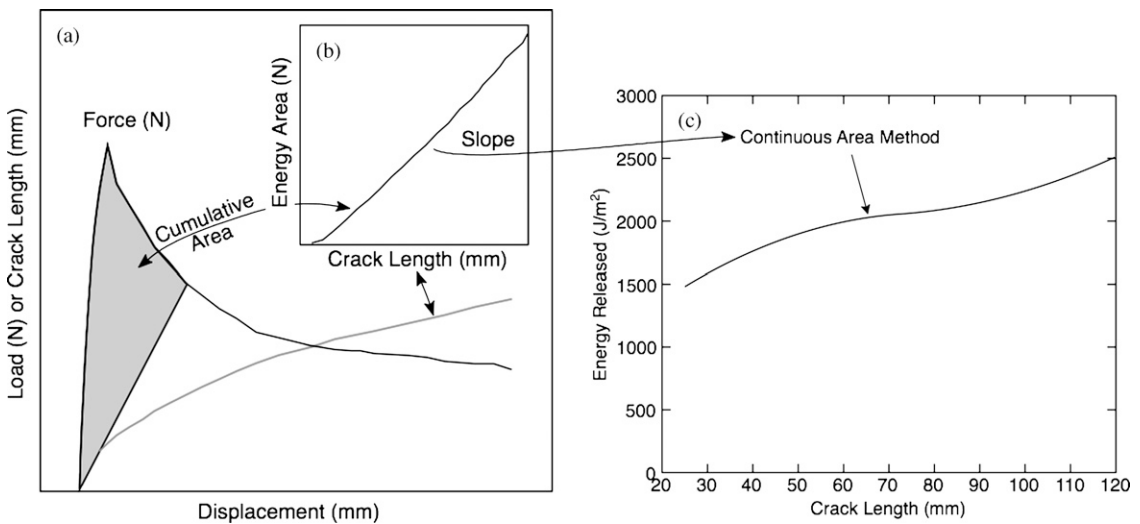


Figure 3. Energy method for measuring  $R$  curve during crack propagation. (a) The experiment is to measure force and crack length as a function of displacement. (b) The shaded cumulative energy area (per unit thickness) is then cross-plotted as a function of crack length. (c)  $R$  curve is slope of that energy plot found by numerical differentiation.

A key requirement of the energy method is accurate crack length measurement during the monotonic tests. For both MDF and PB, the crack tip was difficult to identify visually. This difficulty has led some researchers to define “effective” crack lengths (Ehart et al 1996), but this approach, by definition, means the toughness will be an effective property as well. Fortunately, crack lengths could be measured using DIC (Sutton et al 1983). Specimens were painted with a speckle pattern. During crack propagation, a series of images were recorded. Analysis of these images using DIC methods resolved the axial strain in the crack path. The strain profiles were low far away from the crack tip, but became very high near the crack tip (Matsumoto and Nairn 2009). Although one cannot objectively identify the precise crack tip, these strain profiles retained their shape and simply shifted with the propagating crack. Using the shift in strain field between each image produced accurate measurements of crack growth increments. Crack length was determined by adding these increments to the initial crack length. DIC methods were only needed for MDF and PB cracks. For DF, crack tips could be identified visually; these crack lengths were measured off digital images recorded during tests.

Because of the time-consuming nature of fracture tests, especially when coupled with DIC methods, results reported here are for a single crack propagation experiment in each material and each direction for the various materials.

IB tests were conducted on both commercial and soy PB panels following ASTM (2009b). The IB test is intended to determine tensile strength perpendicular to the plane of the panel. Nine specimens of each type of panel were tested. IB test results were compared with out-of-plane fracture toughness results (ZL and ZT crack growth) to assess each method as a tool for characterizing quality of the internal bonds in the panel.

## RESULTS

### Medium-Density Fiberboard

The MDF results are reported elsewhere (Matsumoto and Nairn 2009). Those experimental results are summarized here for comparison with PB and DF results and analyzed with new modeling (discussed subsequently).  $R$  curves for in-plane cracks (TL and LT) in the 19.05-mm-thick MDF panels are shown in Fig 4 (The 609-kg/m<sup>3</sup> LT directions could not be evaluated because of

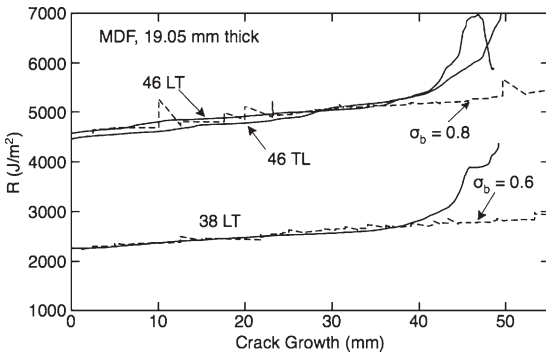


Figure 4. Fracture toughness of two different density medium-density fiberboard (MDF) panels (19.05 mm thick) for in-plane cracks. The dashed lines are numerical models for crack propagation including fiber bridging.

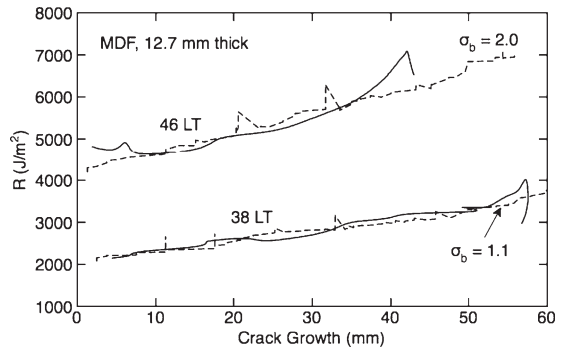


Figure 5. Fracture toughness of two different density medium-density fiberboard (MDF) panels (12.7 mm thick) for in-plane cracks. The dashed lines are numerical models for crack propagation including fiber bridging.

extremely curved cracks.). The denser 737-kg/m<sup>3</sup> panels had about twice the initial toughness of the 609-kg/m<sup>3</sup> panels. Initial toughness is defined as the start of the *R* curve or toughness at the onset of crack growth. After initiation, the toughness increased almost linearly with crack length. The increase was caused by the development of a fiber-bridging zone. The initial specimen with the machined crack had no fiber bridging. As the crack propagated, a zone developed causing the toughness to increase with no indication of reaching a steady state. In some materials, process zones reach a constant or steady-state value and the *R* curve plateaus. In MDF, toughness continued to increase, which implies that the bridging zone continued to develop.

The dashed curves in plots are numerical models of crack propagation including fiber bridging, which are subsequently discussed. Edge effects, which were common near the end of these tests, were an artifact of the data reduction scheme. The final toughness is determined from  $R = dU/da$  where *U* is energy area and *a* is crack length (Fig 3b). Near the end of the test, however, *da* approached zero, which caused *R* to become large and unreliable. All analyses considered only data prior to these rapid rises.

*R* curve results for LT cracks in thin (12.7-mm) MDF panels are given in Fig 5 and can be compared with results for thick (19.05-mm) panels

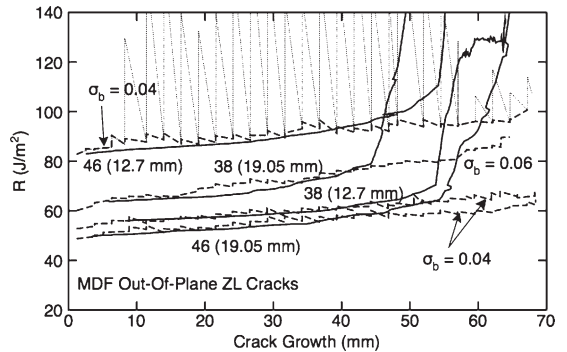


Figure 6. Fracture toughness of two different density and two different thickness medium-density fiberboard (MDF) panels for out-of-plane ZL cracks. The dashed lines are numerical models for crack propagation including fiber bridging.

in Fig 4. The initial MDF toughness was nearly independent of thickness for the range tested here. The thinner panel *R* curves, however, increased faster with crack growth, which probably indicates more effective fiber bridging.

*R* curve results for out-of-plane crack propagation in the ZL direction are shown in Fig 6 (results for ZT cracks were similar and were not plotted). Like in-plane cracks, out-of-plane crack toughness rose linearly during crack growth and never reached steady state. In contrast, initial toughness was about two orders of magnitude lower than in-plane toughness and is now relatively independent of panel density.

Similarly, the magnitude of toughness increase with crack propagation is much lower, indicating less effective fiber bridging. Wood fibers in MDF tend to lie in the plane of the panel and therefore should be less effective at bridging out-of-plane cracks than in-plane cracks.

### Particleboard

$R$  curves for in-plane crack propagation in both commercial and soy PB are shown in Fig 7. The TL and LT directions were uncertain in these panels; these results are thus for generic in-plane cracks. Initial toughness for commercial and soy PB were similar and were two to three times lower than that for MDF at comparable density. As in MDF, PB toughness increased with crack length. In PB, the process zone is bridged by wood particles rather than wood fibers. Compared with soy PB, commercial PB had a slightly higher initial toughness and its  $R$  curve reached a steady state ( $G_{SS}$ ) of about  $2.03 \text{ kJ/m}^2$ . Initial soy PB toughness was slightly lower, but the  $R$  curve continued to rise, never reaching a steady state prior to edge effects. The lower initial toughness of soy PB may be caused by its lower density ( $653 \text{ kg/m}^3$  for soy PB compared with  $730 \text{ kg/m}^3$  for commercial). A slightly larger density difference in MDF panels had a significant effect on in-plane toughness.

The leveling off of toughness for commercial PB indicates a breakdown of the fiber-bridging

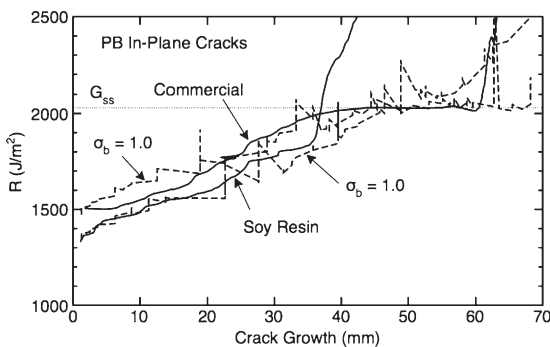


Figure 7. Fracture toughness for in-plane cracks in particleboard (PB) with two different resins. The dashed lines are numerical models for crack propagation including fiber bridging.

zone. In commercial PB, the breakdown begins after about 40 mm of crack growth, which would equate to the length of the bridged zone. For subsequent crack growth, the bridging zone propagates along with the crack, maintaining a nearly constant 40-mm length (Nairn 2009). As a result, the  $R$  curve stays constant and equal to  $G_{SS}$  (Fig 7).

Compared with MDF, out-of-plane crack propagation directions of PB (Fig 8) had higher toughness (1.5-7 times higher), especially for soy PB. These differences were attributed to their differing wood constituents and associated orientations. Wood fibers of MDF tend to lie flat in the plane of the panel and provide little reinforcement in the  $z$  direction. In contrast, PB is composed of wood particles that are more three-dimensional. As evidenced by crack propagation results, these particles bridge cracks better in the  $z$  direction than MDF fibers, which results in higher toughness. Compared with commercial PB, soy PB toughness was about three times higher. Both PB  $R$  curves increased linearly at roughly the same rate. A 3-fold increase in toughness could be caused by resin/wood particle bond differences.

### Douglas-Fir

Crack propagation results for Douglas-fir are shown in Fig 9. Douglas-fir had the lowest in-plane (RL and TL) fracture toughness of all

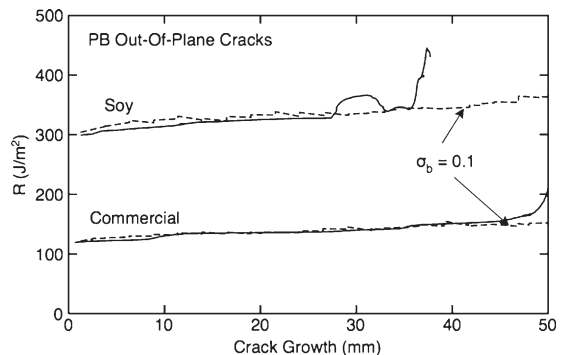


Figure 8. Fracture toughness for out-of-plane cracks in particleboard (PB) with two different resins. The dashed lines are numerical models for crack propagation including fiber bridging.

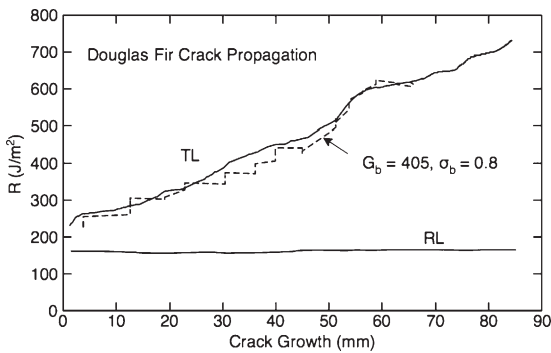


Figure 9. Fracture toughness for TL and RL cracks in Douglas-fir. The dashed line is a numerical model for crack propagation including fiber bridging.

materials tested. The initial toughnesses of the two crack propagation directions (RL and TL) were similar but the curves diverged with crack propagation. During crack propagation, TL direction toughness increased linearly with crack growth, whereas the RL direction remained essentially constant. An increase with crack length in the TL direction can again be attributed to fiber bridging, but now the crack was bridged by nonfractured latewood zones. In contrast, an RL crack can find a path mostly through early wood, which apparently fractures with little material remaining to bridge the crack. This conclusion is supported by observations of the fracture surfaces. The TL fracture surface was rough with ridges at latewood zones that had bridged the crack plane. In contrast, the RL fracture surface was very smooth because little wood material bridged the crack plane.

### Internal Bond Tests

A common way to assess PB and resin quality is through the IB test (ASTM 2009b). In an IB test, a 25.4 × 25.4-mm block is glued to end blocks and loaded in transverse tension. To compare IB results with these new out-of-plane fracture results, IB tests were run on the same panels tested for fracture. IB strength for commercial PB was 0.43 MPa with a coefficient of variation (COV) of 10.7%. For soy PB, IB strength was 0.52 MPa with a COV of 17.8%. The soy panel

had a slightly higher value even with its lower panel density, but the relative difference between the two was small compared with the difference in their fracture toughness values. In other words, IB results barely distinguished the two materials whereas fracture results identified a clear distinction that suggests soy PB panels are significantly better with three times higher toughness.

### Crack Propagation Modeling and Discussion

Fracture mechanics standards (ASTM 2006) and most prior work on wood (Johnson 1973; Schniewind and Centeno 1973) emphasize fracture toughness at initiation of crack growth. In materials that develop process zones, this approach misinterprets the fracture properties of the materials. It discards all of the interesting effects that occur during crack propagation. For example, initiation toughness in bone is exceedingly small, but its  $R$  curve rises rapidly during crack growth (Nalla et al 2005). Based on its initiation toughness, bone would be characterized as an unsuitable structural material. Fortunately, its full fracture behavior is much better.

As in bone, most wood composites and solid wood display rising  $R$  curves. The implication is that initiation of fracture, as commonly studied in the past, may be insufficient to gain a full understanding of the fracture properties of wood. This situation is remedied by extending initiation experiments to the propagation phase and monitoring changes in toughness caused by process zones. Changes were manifested here by rising  $R$  curves. Because all curves were nearly linear in crack growth, the  $R$  curves can be described by initiation toughness,  $G_{init}$ , and  $R$  curve slope. Experimental results for these values are listed in Table 1. Only one crack path (RL fracture in DF) had zero slope. For most materials, the  $R$  curve continued to rise for the entire test, which suggests the potential bridging zone was large—larger than the specimen sizes used. One material appeared to reach steady-state toughness (in-plane commercial PB), and one material had no rising  $R$  curve and therefore was always at steady state (DF in the RL direction). The

Table 1. Experimental and simulation results for fracture properties of medium-density fiberboard (MDF), particleboard (PB), and Douglas-fir (DF).<sup>a</sup>

Material	Crack	Thickness (mm)	$G_{init}$ (J/m <sup>2</sup> )	$R$ slope (J/m <sup>2</sup> /mm)	$\sigma_b$ (MPa)	$G_b$ (J/m <sup>2</sup> )	$\delta_c$ (mm)
MDF 38	LT	19.05	2230	10.00	0.60	>450	>1.5
	LT	12.70	2048	19.60	1.10	>1182	>2.2
	Z	19.05	59	0.35	0.06	>16	>0.5
	Z	12.70	52	0.25	0.04	>12	>0.6
MDF 46	LT	19.05	4550	18.00	0.80	>650	>1.6
	TL	19.05	4450	18.00	0.80	>750	>1.9
	LT	12.70	4150	60.00	2.00	>1950	>2.0
	TL	12.70	4000	60.00	4.00	>3000	>1.5
	Z	19.05	48	0.22	0.04	>11	>0.5
	Z	12.70	82	0.26	0.04	>12	>0.6
	Z	12.70	82	0.26	0.04	>12	>0.6
PB commercial	LT/TL	19.48	1460	16.60	1.00	=570	=1.2
	Z	19.48	120	0.72	0.10	>31	>0.6
PB soy	LT/TL	19.43	1330	14.20	1.00	>490	>1.0
	Z	19.43	300	1.25	0.10	>45	>0.9
DF	TL	22.23	215	6.10	0.80	>400	>1.0
	RL	22.60	158	0.09	0.00	=0	=0

<sup>a</sup>  $G_{init}$  and  $R$  slope come from experimental results;  $\sigma_b$  are results of simulations;  $G_b$  and  $\delta_c$  are bounds on those properties based on experimental and simulation results (if listed with >) or measured value (if listed with =).

bridging toughness values for these materials are indicated in Table 1. Bridging toughness is the difference between steady-state toughness,  $G_{ss}$ , and initiation toughness,  $G_{init}$ , or  $G_b = G_{ss} - G_{init}$ .

To extract material properties from these data, the slopes should be interpreted in terms of stresses carried by the bridging zone. This analysis

requires numerical modeling of crack growth with fiber bridging, such as described in Nairn (2009). First, the CT specimens were discretized into material points using the material point method (MPM) (Sulsky et al 1994) (Fig 10a). The particles were evenly spaced and separated by 0.635 mm (this resolution was verified for convergence). An initial crack was inserted using

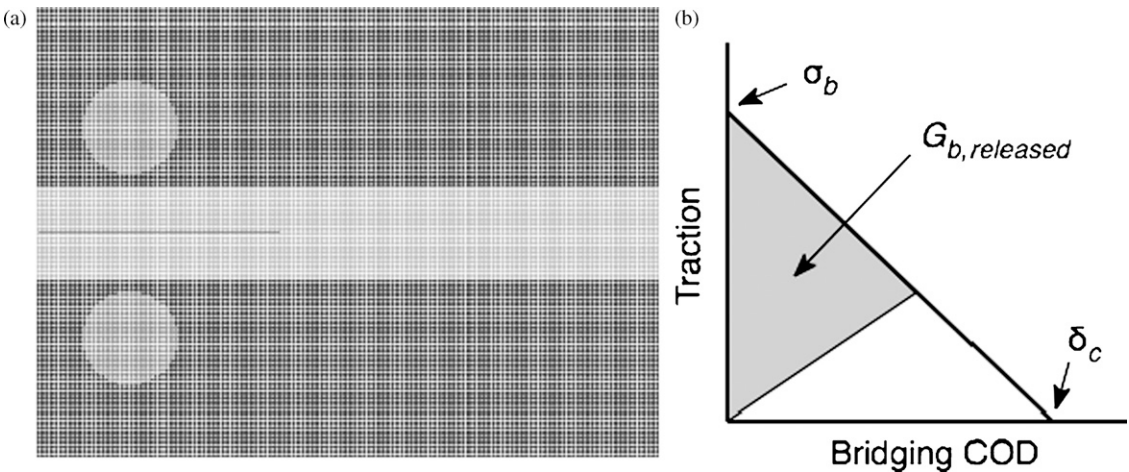


Figure 10. (a) Material point method model for compact tension specimens. The dark line in the middle is the initial crack. The round pins are steel. The central area is identical to rest of panel for in-plane cracks but has Z-slice properties for out-of-plane cracks. (b) A pure linear-softening traction law, which is linear from peak bridging stress,  $\sigma_b$ , to critical crack opening displacement,  $\delta_c$ .

explicit crack methods for MPM (Nairn 2003). The loading pins were modeled as steel cylinders and set to move at constant velocity in the opening direction. Loads were transferred from the pins to the CT specimen by frictionless contact (Bardenhagen et al 2001; Lemiale et al 2010). For in-plane cracks, all material points in the specimen were the same. For out-of-plane cracks, the material points in the center of the specimen were set to the properties of the  $z$ -crack slice, whereas the remaining particles used the in-plane properties for the same material.

Next, at each time step, the  $J$  integral was calculated (by methods that account for the fiber-bridging zone [Nairn 2009]) and then compared with  $G_{init}$ , where  $G_{init}$  was determined from experiments. Whenever  $J > G_{init}$ , the crack tip propagated the distance of one particle spacing (0.635 mm). In the wake of the crack propagation, a traction law was assigned between the two crack surfaces. The traction law was assumed to be linear softening (Fig 10b), in which the traction decreased linearly from peak bridging stress,  $\sigma_b$ , to zero at the critical crack opening displacement (COD),  $\delta_c$ , where the fibers fail and the bridging zone starts to break down. The area under the traction law,  $G_b = \sigma_b \delta_c/2$ , is total toughness associated with bridging. The linear softening law was selected because it has been associated with linearly increasing  $R$  curves (Lindhagen and Berglund 2000; Nairn 2009).

This progressive failure analysis continued until the crack tip reached the end of the specimen. The  $R$  curve was calculated each time the crack propagated as  $R = G_{init} + G_{b,released}$ , where  $G_{b,released}$  is energy released by the entire bridging zone during the last increment in crack growth. This energy can be found from the shaded area under the traction law up to the current crack opening displacement at the opened edge of the bridging zone as indicated in Fig 10b (Nairn 2009). Finally, this  $R$  curve was output as a function of crack growth and compared with experimental results. The traction law properties were varied until modeling matched experiments. Because few results reached steady state, the only traction law property that could be

determined was  $\sigma_b$ , but it could be determined without needing to know  $G_b$  or  $\delta_c$ .

The other mechanical properties necessary for simulations were also obtained from fracture tests. The in-plane CT moduli were assumed to be isotropic and were found by matching experimentally observed specimen stiffness to a finite element calculation of that stiffness as a function of panel modulus. The panel parts of the out-of-plane CT specimens were also assumed isotropic and used the stiffness from in-plane tests, but the cores (central regions) were assumed to be transversely isotropic. The axial direction of the core was in the  $y$  direction, and it represents the through-the-thickness modulus of MDF or PB. The modulus in the  $x$  direction was assumed to be the same as the panel modulus from in-plane experiments. The axial shear modulus was assumed to be two-thirds of the axial modulus. Thus, the only unknown modulus was the  $y$  direction modulus. It was found by matching experimentally observed CT specimen stiffness to finite element calculations. Finally, DF was assumed to have typical orthotropic properties (Bodig and Jayne 1982). These values gave reasonable results for CT specimen stiffness. All assumed mechanical properties are given in Table 2. The resulting  $R$  curves were relatively insensitive to these specific values. The  $R$  curves depended much more on assumed fracture properties and traction law properties.

All experimental results were fit to MPM modeling simulations to find  $\sigma_b$ ; if possible, the fit also found  $G_b$ . The resulting fits are plotted in Figs 4-9; the numerical results are in Table 1. MPM results fit the experiments well but had some noise. The noise was believed to be a consequence of dynamic fracture simulations. Whenever a computer simulation propagates cracks (by releasing elements in finite element analysis or by extending an explicit crack in MPM), the object will release energy. This propagation is meant to model crack propagation in real materials, but the real material absorbs that energy while creating the new surface area. In elastic simulations, however, there is no mechanism for absorbing released energy. As a consequence,

Table 2. Mechanical properties calculated from compact tension specimens and used in all plotted simulations.<sup>a</sup>

Material <sup>b</sup>	Thickness (mm)	$E$ (MPa)	$E_A$ (MPa)	$G$ (MPa)	$\nu$
MDF 38	19.05	1350			
MDF 38	12.7	1185			
MDF 38 Z	19.05	1350	90	$G_A = 60$	$\nu_A = 0.1$ $\nu_T = 0.33$
MDF 46	19.05	2190			
MDF 46	12.7	2600			
MDF 46 Z	19.05	2190	200	$G_A = 100$	$\nu_A = 0.1$ $\nu_T = 0.33$
PB Comm	19.48	1785			
PB Comm Z	19.48	1785	220	$G_A = 140$	$\nu_A = 0.1$ $\nu_T = 0.33$
PB Soy	19.43	2016			
PB Soy Z	19.43	2016	90	$G_A = 55$	$\nu_A = 0.1$ $\nu_T = 0.33$
DF	22.23	14500	$E_{RR} = 960$ $E_{TT} = 620$	$G_{LR} = 830$ $G_{LT} = 760$ $G_{RT} = 80$	$\nu_{LT} = 0.42$ $\nu_{LR} = 0.37$ $\nu_{TR} = 0.35$

<sup>a</sup> For isotropic properties, the  $E$  column gives the modulus. For transversely isotropic Z slices,  $E$  gives modulus in the  $x$  direction. The  $y$  direction modulus, axial direction is given in the  $E_A$  column. For DF,  $E$  gives longitudinal modulus and other columns give all other orthotropic properties.

<sup>b</sup> MDF = medium-density fiberboard; PB = particleboard; Comm = commercial; DF = Douglas-fir.

the released energy becomes kinetic energy. This kinetic energy, which is localized at the crack tip, can induce oscillations in  $J$  integral calculations at the crack tip, which sometimes necessitates artificial damping. Here, the oscillations were normally small and no damping was used. They were kept small by decreasing loading rate. All simulations used a loading rate of 1 m/s, which was much faster than experiments but small enough to avoid inertial effects and to minimize kinetic energy oscillations. The oscillations were similar in magnitude for out-of-plane cracks, but because the energy released was much smaller, they looked larger. Figure 6 shows one fit with all oscillations. Kinetic energy artifacts caused the simulated  $R$  curve to periodically overshoot the expected  $R$  curve for very short intervals (one or two time steps). The oscillations, however, were bounded on the bottom by the simulated  $R$  curve. Thus, for all out-of-plane simulations, the transient high points were removed and the plotted simulations were the envelope for the lower bound of the output results. The in-plane results plotted the full  $R$  curves with all oscillations. These oscillations had nothing to do with MPM. They were a natural consequence of any computational mechanics simulation that conserves energy while dynamically introducing crack extensions.

## Medium-Density Fiberboard and Particleboard

Bridging stresses for in-plane cracks in  $\approx 19$ -mm-thick MDF 38, MDF 46, and PB (both resins) were 0.6, 0.8, and 1.0 MPa, respectively. A comparison of MDF 38 to MDF 46 shows that the denser panel had higher bridging stress, probably because the denser panel had more fibers per unit area. Comparing MDF with PB shows that PB had slightly higher bridging stress. The coarse particles in the center of PB were more effective at bridging than the fine fibers in MDF. For thinner panels (12.7 mm), the denser MDF 46 had higher bridging stress than MDF 38. Compared with thicker panels, the bridging stress for the thinner MDF panels was higher; it ranged from 1.1 to 4.0 MPa. Perhaps the manufacturing process of the thinner panels did a better job of aligning fibers in the plane of the panels. The better the fibers lie in the plane of a panel, the more effective they should be at bridging in-plane cracks.

Bridging stresses for out-of-plane cracks were all about an order of magnitude lower than for in-plane cracks. Apparently, the panel structure promotes bridging of in-plane cracks but inhibits bridging of out-of-plane cracks. For MDF, in particular, the predominantly in-plane fibers were

parallel to out-of-plane cracks and thus very ineffective at carrying bridging stress. As with in-plane cracks, the bridging stress for out-of-plane cracks in PB was higher than for MDF, probably for the same reasons.

Because crack propagation rarely reached steady state, the only traction law parameter that could be measured was bridging stress. Although neither  $G_b$  nor  $\delta_c$  could be measured, those properties could be bounded. The  $G_b$  column in Table 1 has a lower bound to  $G_b$  calculated from the maximum observed  $R$  curve prior to edge effects. This result is a lower bound because the actual  $G_b$  would be higher if crack propagation could have been extended to steady state. By using the relation  $G_b = \sigma_b \delta_c/2$ , a lower bound for  $G_b$  leads to a lower bound for bridging COD:  $\delta_c \geq 2G_b/\sigma_b$  (Table 1). For in-plane cracks,  $\delta_c$  was about 1-2 mm, which is similar to dimensions of wood elements (eg longitudinal tracheids (Bowyer et al 2007) or particles) in MDF or PB and reinforces the argument that the rising  $R$  curve was related to bridging of these elements across the crack surface. The critical CODs for the out-of-plane cracks were  $<1$  mm. One interpretation is that the fibers or particles tend to lie closer to the plane of the panel and thus are easier to pull out in the thickness direction.

The crack plane for out-of-plane fracture tests was the same as the failure plane in IB tests. As a consequence, the out-of-plane fracture test might be a candidate for a new test that can replace IB testing. Most areas of material science identify fracture toughness as a more fundamental material property (Williams 1984). IB tests were performed on the same PB panels tested by crack propagation. The IB results suggest that commercial and soy panels were of similar quality (producing similar failure stresses within similar COV), whereas the fracture results suggest that the soy resin panel was significantly better. Unfortunately, no COV for fracture tests could be assessed because only one test was performed for each material because of its time-consuming nature. In general, however, fracture tests have less scatter than strength tests. In fracture tests, the crack is forced to propagate from a well-

controlled crack tip. In strength tests, failure occurs at statistically random locations resulting in much higher scatter. Furthermore, a single fracture test (as performed in this study) gives a full  $R$  curve and thus provides more information than a single value obtained in other tests. The question remains, which test is a better measure of quality? Can fewer but more time-consuming fracture tests lead to better products than many highly scattered IB tests? These results suggest that out-of-plane fracture testing might identify differences in panels that are not evident in IB testing. Those differences might translate to improved panels if used to guide new materials development.

### Douglas-Fir

DF fracture results showed a dramatic difference between TL and RL fracture, but that difference was only observed by monitoring crack propagation. Most prior fracture work on DF (and some other species) focused on initiation. The results vary and interpretations are misguided because they are based on incomplete fracture information. Two prior initiation studies used conventional fracture methods to measure critical stress intensity factors,  $K_{Ic}$ , for both TL and RL fracture of DF. Schniewind and Centeno (1973) found  $K_{Ic}$  of 0.409 MPa  $\sqrt{m}$  for RL fracture and 0.309 MPa  $\sqrt{m}$  for TL fracture. They concluded the differences were significant and “could be attributed to rays acting as crack arrestors in the RL system, whereas in the TL system, the cracks can run along the rays.” Johnson (1973) found  $K_{Ic}$  of 0.324 MPa  $\sqrt{m}$  for RL fracture and 0.374 MPa  $\sqrt{m}$  for TL fracture. Here the ranking of TL and RL toughness was switched, but they concluded fracture properties for these two directions were indistinguishable.

To compare our new energy method with prior  $K_{Ic}$  results, prior toughnesses must be converted to toughness as energy release rates. The conversion for orthotropic materials (Kanninen and Popelar 1985) is

$$G_{Ic} = \frac{K_{Ic}^2}{E_{eff}} \quad (1)$$

where the effective modulus,  $E_{eff}$ , depends on the crack plane. For RL fracture

$$\frac{1}{E_{eff}} = \sqrt{\frac{1}{2E_{LL}E_{RR}} \left( \frac{\sqrt{E_{LL}}}{E_{RR}} + \frac{E_{LL}}{2G_{LR}} - \nu_{LR} \right)^2} \quad (2)$$

For TL fracture

$$\frac{1}{E_{eff}} = \sqrt{\frac{1}{2E_{LL}E_{TT}} \left( \frac{\sqrt{E_{LL}}}{E_{TT}} + \frac{E_{LL}}{2G_{LT}} - \nu_{LT} \right)^2} \quad (3)$$

Using DF properties in Table 2,  $E_{eff}$  values for RL and TL fracture are 1.507 and 1.135 GPa, respectively. Schniewind and Centeno (1973) results for  $G_{Ic}$  are 111 J/m<sup>2</sup> for RL fracture and 84 J/m<sup>2</sup> for TL fracture. Johnson (1973) results for  $G_{Ic}$  are 70 J/m<sup>2</sup> for RL fracture and 123 J/m<sup>2</sup> for TL fracture. These results are similar to initiation values measured by the energy method, but propagation results show that TL was tougher. This new fracture information shows that ray cells played little or no role in DF fracture. Ray cells were certainly neither arresting nor bridging the RL fracture surface.

Two other studies used wedge specimens and found toughness from work of fracture or total area under the load deflection curve (although for species different from DF) (Fruhmann et al 2002; Reiterer et al 2002a, 2002b). In theory, this approach measures average toughness that includes effects of crack propagation. It is uncertain, however, how it might be influenced by specimen shape or edge effects. Furthermore, they measured only a single toughness rather than a full  $R$  curve. The findings of these two studies differed. Fruhmann et al (2002) found the TL toughness was higher than the RL toughness in both spruce and beech. They concluded that latewood material enhanced TL toughness. Reiterer et al (2002a, 2002b) observed RL toughness higher than TL toughness in spruce, alder, oak, and ash. They attributed the difference to ray cells, particularly in the hardwood species. As in initiation methods, interpretation

of total fracture work as a single toughness ignores much of the fracture information. Average toughness, at best, is a sum of initiation and average bridging toughness over the length of the specimen. No specific fiber-bridging properties are measured. The full characterization of the fracture toughness of solid wood or wood composites is best characterized by monitoring toughness as a function of crack growth. When investigating differences among species, crack planes, and wood products, it is preferable to base conclusions on the full  $R$  curve instead of the partial information provided by other tests.

#### ACKNOWLEDGMENTS

This work was supported, in part, by a grant from the US Department of Agriculture, Cooperative State Research, Education, and Extension Service (2008-35504-19227).

#### REFERENCES

- ASTM (2006) E399-05a. Standard test method for plane-strain fracture toughness of metallic materials. American Society for Testing and Materials, West Conshohocken, PA.
- ASTM (2009a) D 3043-00. Standard test methods for structural panels in flexure. American Society for Testing and Materials, West Conshohocken, PA.
- ASTM (2009b) D 1037-06a. Standard test methods for evaluating properties of wood-base fiber and particle panel materials. American Society for Testing and Materials, West Conshohocken, PA.
- Atkins AG, Mai YW (1985) Elastic and plastic fracture. John Wiley & Sons, New York, NY.
- Bardenhagen SG, Guilkey JE, Roessig KM, Brackbill JU, Witzel WM, Foster JC (2001) An improved contact algorithm for the material point method and application to stress propagation in granular material. *Comput Model Eng Sci* 2:509-522.
- Bodig J, Jayne BA (1982) Mechanics of wood and wood composites. Van Nostrand-Reinhold Co., Inc., New York, NY.
- Bowyer JL, Shmulsky R, Haygreen JG (2007) Forest products and wood science, an introduction, fifth edition. Blackwell Publishing, Ames, IA.
- Ehart RJA, Stanzl-Tschegg SE, Tschegg EK (1996) Characterization of crack propagation in particleboard. *Wood Sci Technol* 30:307-321.
- Fruhmann K, Reiterer A, Tschegg EK, Stanzl-Tschegg SS (2002) Fracture characteristics of wood under mode I,

- mode II and mode III loading. *Philos Mag A* 82(17-18): 3289-3298.
- Johnson JA (1973) Crack initiation in wood plates. *Wood Sci* 6(2):151-158.
- Kanninen MF, Popelar CH (1985) *Advanced fracture mechanics*. Oxford University Press, New York, NY. 41 pp.
- Lemiale V, Nairn JA, Hurman A (2010) Simulation of equal channel angular pressing with the material point method. *Comput Model Eng Sci* 70(1):41-66.
- Li K, Peshkova S, Geng X (2004) Investigation of soy protein-kymene adhesive systems for wood composites. *J Am Oil Chem Soc* 81(5):487-491.
- Lindhagen JE, Berglund LA (2000) Application of bridging-law concepts to short-fibre composites Part 1: DCB test procedures for bridging law and fracture energy. *Comp Sci Technol* 60:871-883.
- Matsumoto N, Nairn JA (2009) The fracture toughness of medium density fiberboard (MDF) including the effects of fiber bridging and crack-plane interference. *Eng Fract Mech* 76:2748-2757.
- Nairn JA (2003) Material point method calculations with explicit cracks. *Comput Model Eng Sci* 4:649-664.
- Nairn JA (2009) Analytical and numerical modeling of R curves for cracks with bridging zones. *Int J Fract* 155:167-181.
- Nalla RK, Kruzic JJ, Kinney JH, Ritchie RO (2005) Mechanistic aspects of fracture and R-curve behavior in human cortical bone. *Biomaterials* 26(2):217-231.
- Reiterer A, Burgert I, Sinn G, Tschegg S (2002a) The radial reinforcement of the wood structure and its implication on mechanical and fracture mechanical properties—A comparison between two tree species. *J Mater Sci* 37(5):935-940.
- Reiterer A, Sinn G, Stanzl-Tschegg S (2002b) Fracture characteristics of different wood species under mode I loading perpendicular to the grain. *Mat Sci Eng A-Struct* 332(1-2):29-36.
- Schniewind AP, Centeno JC (1973) Fracture toughness and duration of load factor I. Six principal systems of crack propagation and the duration factor for cracks propagating parallel to grain. *Wood Fiber Sci* 5:152-159.
- Sulsky D, Chen Z, Schreyer HL (1994) A particle method for history-dependent materials. *Computer Methods in Applied Mechanics and Engineering* 118(1):179-186.
- Sutton MA, Wolters WJ, Peters WH, Rawson WF, McNeil SR (1983) Determination of displacement using an improved digital image correlation method. *Image Vis Comput* 1(3): 133-139.
- Williams JG (1984) *Fracture mechanics of polymers*. John Wiley & Sons, New York, NY.